2016

Concerted Hydrogen-Bond Breaking by Quantum Tunneling in the Water Hexamer Prism

Jeremy O. Richardson
University of Cambridge

Cristobal Perez
University of Virginia

Simon Lobsiger
University of Virginia

Adam A. Reid
University of Cambridge

Berhane Temelso
bt018@bucknell.edu

See next page for additional authors

phase, respectively (*12*), indicating that the faces of the walls were the (010) planes. The anion sublattice viewed over the face of the RD Cu_2O NC displayed a twofold symmetry (AB stacking), with a bcc structure (Fig. 4D). The anion sublattice of the (010) face of the RD $Cu_{1.75}S$ nanocage displayed a superimposed pseudohexagonal symmetry—more precisely, C_2 symmetry (ABA′B′ stacking), with an hcp-like structure (Fig. 4E).

The similarities between the surface anion sublattice symmetries and stacking way indicated that it was possible to transform the crystal structure from a cubic Cu_2O to triclinic $Cu_{1.75}S$ structure via anion-exchange reaction while maintaining the shape. The pseudohexagonal symmetry of the anion sublattice in $Cu_{1.75}S$ was similar to that of a hexagonally symmetrical (0001) plane (AB stacking) of a wurtzite structure. Thus, RD CdS nanocages with a wurtzite structure could be formed by further cation-exchange reaction of the RD $Cu_{1.75}S$ nanocages even at ambient temperature (Fig. 4F). The HR-TEM image of the RD CdS nanocage (Fig. 3L) displayed lattice fringe spacing of 0.36 and 0.21 nm, corresponding to $(10\bar{1}0)$ and $(11\bar{2}0)$ lattice planes of a wurtzite CdS nanocage, respectively. The crystallographic relation between the neighboring walls of the RD nanocages was determined from the FFT patterns of the faces and sides of the walls (Fig. 4, E and F). Similar to the RH nanocages, the RD nanocages were also composed of crystallographically independent or polycrystalline walls, induced by the pseudomorphic transformation in anion-exchange reaction. The connection between neighboring walls is depicted schematically in fig. S2B. The lattice stacking way (AB) of the walls was also unchanged after the ion-exchange reactions (Fig. 4, D to F). Although the anion sublattices of the $Cu_{1.75}S$ nanocage in layer A′ and B′ are slightly distorted (fig. S3), the symmetry of the anion sublattices still closely resembles the layers A and B. In addition, the volumes of the ion-exchanged products expanded because of the larger radii of S^{2-} and Cd^{2+} (table S1) (*20*).

One of the advantages of this phase-transition method is to selectively obtain polymorphic crystal phases at ambient conditions. The phase transition from a zincblende to wurtzite structure of ZnS takes place at 1020°C. With this phase transition method, ZnS with a zincblende and a wurtzite phase could both be obtained, even at room temperature. We conducted the pseudomorphic transformation of the RH and RD Cu_2O to Cu_xS and further to ZnS under ambient conditions. The SEM and TEM images of the resulting ZnS nanocages are shown in fig. S4A. Similar to the case of the CdS nanocages, subsequent cation exchange reactions of RH $Cu_{1.8}S$ and RD $Cu_{1.75}S$ nanocages with Zn^{2+} are likely to give the zincblende RH ZnS and the wurtzite RD ZnS nanocages, respectively (fig. S4B). The UV-Vis-NIR spectra displayed the characteristic semiconducting ZnS phase (fig. S4C) but showed weakly localized surface plasmon resonance peaks in both ZnS nanocages, indicating that small amounts of the Cu_xS phases were present (*21*). The complete cation exchange did not proceed, but we could demonstrate the potential of our method to produce the unobtainable crystal phases under ambient conditions.

We emphasize that the validity of our observation is strongly supported by the previous report (*4*) that demonstrated an anion exchange of the hexagonal pyramid–shaped ZnO NCs with a wurtzite phase to the ZnS hollow NCs with a wurtzite phase. We envisage that this pseudomorphic transformation method could be applicable to a number of other ionic NCs at ambient temperatures, even if they are high-temperature stable phases such as wurtzite ZnS.

REFERENCES AND NOTES

1. G. D. Moon *et al.*, *Nano Today* **6**, 186–203 (2011).
2. M. Saruyama *et al.*, *J. Am. Chem. Soc.* **133**, 17598–17601 (2011).
3. T. Teranishi, M. Sakamoto, *J. Phys. Chem. Lett.* **4**, 2867–2873 (2013).
4. J. Park, H. Zheng, Y. W. Jun, A. P. Alivisatos, *J. Am. Chem. Soc.* **131**, 13943–13945 (2009).
5. P. K. Jain, L. Amirav, S. Aloni, A. P. Alivisatos, *J. Am. Chem. Soc.* **132**, 9997–9999 (2010).
6. H. Li *et al.*, *Nano Lett.* **11**, 4964–4970 (2011).
7. D. Zhang *et al.*, *J. Am. Chem. Soc.* **136**, 17430–17433 (2014).
8. D. H. Son, S. M. Hughes, Y. Yin, A. Paul Alivisatos, *Science* **306**, 1009–1012 (2004).
9. R. D. Robinson *et al.*, *Science* **317**, 355–358 (2007).
10. W. C. Huang, L. M. Lyu, Y. C. Yang, M. H. Huang, *J. Am. Chem. Soc.* **134**, 1261–1267 (2012).
11. C. H. Kuo, M. H. Huang, *J. Phys. Chem. C* **112**, 18355–18360 (2008).
12. W. G. Mumme, R. W. Gable, V. Petricek, *Can. Mineral.* **50**, 423–430 (2012).
13. S. B. Qadri *et al.*, *J. Appl. Phys.* **89**, 115–119 (2001).
14. Z. Wang *et al.*, *Nat. Mater.* **4**, 922–927 (2005).
15. S. B. Qadri *et al.*, *Phys. Rev. B* **60**, 9191–9193 (1999).
16. Materials and methods are available as supplementary materials on *Science* Online.
17. C. H. Kuo, Y. T. Chu, Y. F. Song, M. H. Huang, *Adv. Funct. Mater.* **21**, 792–797 (2011).
18. M. Kanehara, H. Arakawa, T. Honda, M. Saruyama, T. Teranishi, *Chem. Eur. J.* **18**, 9230–9238 (2012).
19. C. H. Kuo, C. H. Chen, M. H. Huang, *Adv. Funct. Mater.* **17**, 3773–3780 (2007).
20. J. B. Rivest, P. K. Jain, *Chem. Soc. Rev.* **42**, 89–96 (2013).
21. D. H. Ha *et al.*, *Nano Lett.* **14**, 7090–7099 (2014).
22. W. W. Yu, X. Peng, *Angew. Chem. Int. Ed. Engl.* **41**, 2368–2371 (2002).

ACKNOWLEDGMENTS

This work was partly supported by the Artificial Photosynthesis Project (ARPChem) of the New Energy and Industrial Technology Development Organization (NEDO) of Japan.

SUPPLEMENTARY MATERIALS

www.sciencemag.org/content/351/6279/1306/suppl/DC1
Materials and Methods
Figs. S1 to S4
Table S1

29 September 2015; accepted 1 February 2016
10.1126/science.aad5520

HYDROGEN BONDING

Concerted hydrogen-bond breaking by quantum tunneling in the water hexamer prism

Jeremy O. Richardson,[1,2]* Cristóbal Pérez,[3]† Simon Lobsiger,[3] Adam A. Reid,[1]‡ Berhane Temelso,[4] George C. Shields,[4] Zbigniew Kisiel,[5] David J. Wales,[1] Brooks H. Pate,[3]* Stuart C. Althorpe[1]*

The nature of the intermolecular forces between water molecules is the same in small hydrogen-bonded clusters as in the bulk. The rotational spectra of the clusters therefore give insight into the intermolecular forces present in liquid water and ice. The water hexamer is the smallest water cluster to support low-energy structures with branched three-dimensional hydrogen-bond networks, rather than cyclic two-dimensional topologies. Here we report measurements of splitting patterns in rotational transitions of the water hexamer prism, and we used quantum simulations to show that they result from geared and antigeared rotations of a pair of water molecules. Unlike previously reported tunneling motions in water clusters, the geared motion involves the concerted breaking of two hydrogen bonds. Similar types of motion may be feasible in interfacial and confined water.

In addition to its bulk phases, water can form small gas-phase clusters $(H_2O)_n$, in which the molecules are held together by a network of hydrogen bonds. The cluster dynamics can be probed by high-resolution rovibrational spectroscopy (*1–9*) and interpreted by theoretical simulations (*10–27*). The nature of the interactions between the water molecules is the same in the clusters as in the bulk (many-body forces beyond the three-body term are relatively weak) (*28*), and hence the cluster spectra can be used to test universal models (*25, 29–32*) of the water intermolecular potential energy surface, giving insight into hydrogen bonding in all phases of water. At low temperatures, the molecules are frozen into a network and can only rearrange by quantum tunneling, which causes splittings in the spectrum ranging from megahertz to terahertz (*33*). Quantum simulations (*10–27*) have identified rearrangements that involve free hydrogen flips that break no

hydrogen bonds, and bifurcations that break one bond (*2*).

Here we report observation of a tunneling motion that concertedly breaks two hydrogen bonds in a water cluster. The hexamer is the smallest cluster with a branched three-dimensional equilibrium geometry (*5*) and has thus been dubbed the smallest droplet of water. It has a variety of isomers (*12–14*, *21*, *34–36*), of which the spectrum of the lowest-energy prism isomer, PR1 of Fig. 1 (see the supplementary materials for a discussion of other prism isomers), was recently found to show a splitting pattern, which was attributed to tunneling (*6*). Here we report new measurements and quantum simulations on PR1 that uncover the dynamics responsible for the splittings.

Tunneling in water clusters occurs when the molecules in their equilibrium geometry rearrange to produce an equivalent structure, by permuting equivalent atoms or inverting the structure through its center of mass. These geometrically identical structures (which can be distinguished only by labeling the atoms and specifying the chirality) are termed versions. The number of versions is equal to the size of the group of all nuclear permutations and inversions (*37*), which for PR1 gives an enormous total of $2 \times 6! \times 12! \simeq 10^{12}$. However, only versions linked by short and energetically accessible tunneling pathways produce observable splittings. We therefore need to consider only pathways that rotate the water molecules within the structure, because these avoid breaking covalent bonds. For smaller clusters, these rules are sufficient to assign tunneling splittings (*2*, *15*, *16*, *20*, *27*). However, for PR1, the size of the space left to explore is still vast.

To narrow down further the number of likely tunneling pathways, we measured the rotational spectra of all 64 isotopologs of the hexamer PR1 prism with the formula $(H_2{}^{18}O)_n(H_2{}^{16}O)_{6-n}$ ($n = 0 \ldots 6$); these are presented in tables S5 to S68. Figure 2A shows the tunneling patterns for three *a*-type rotational transitions of the $(H_2{}^{16}O)_6$ cluster. These spectra show the characteristic splitting pattern previously observed (*6*). Isotopic substitution destroys this pattern, except in $(H_2{}^{18}O)_6$ and in the six doubly substituted isotopologs shown in Fig. 2B. This tells us immediately that the tunneling paths must rearrange two separate water molecules in the structure, ruling out motions such as the flip and bifurcation observed in other water clusters (*2*, *15*, *16*, *20*, *27*). Closer inspection shows that the observed splitting is slightly reduced when the A+D dimer is substituted with the heavier isotope; the composition of the remaining tetramer portion of the cluster does not affect the splitting. The tunneling motion must therefore involve rearrangements of molecules A and D, and the dynamics are probably localized in this part of the cluster.

To elucidate the dynamics further, it was necessary to carry out quantum simulations on an accurate potential energy surface. Full quantum calculations are impossible for this 48-degrees-of-freedom problem, so we used the ring-polymer instanton (RPI) method (*27*, *38*, *39*). This method assumes that the tunneling can be approximated by fluctuations around the minimum-action or instanton paths connecting different versions (*40*). The instanton path is found by minimizing the potential energy of a fictitious polymer formed by linking replicas of the system by harmonic springs. Previous studies on other water clusters (*27*, *39*) have shown that this method correctly predicts the pattern and order of magnitude of the tunneling splittings and that the instanton paths give a useful representation of the tunneling dynamics. Further details of the RPI method are given in the supplementary materials. The potential energy surface used was the HBB2-pol surface (*31*); we also made comparisons with the MB-pol surface (*32*) and found no major qualitative differences in the results (table S1).

Because the space of possible tunneling paths is vast, it is necessary to have an idea of the starting path, which can then be refined using the RPI method. Initially, we considered paths that resemble the flip motions observed in other water clusters, which involve the wag of a non–hydrogen-bonded H atom. No single flip connects versions in the hexamer prism, but a double flip corresponding to the permutation $P_a = (AD)(BF)(CE)(1\,7)(2\,8)(3\,11)(4\,12)(5\,9)(6\,10)$ (using the labeling in Fig. 1) does. The resulting instanton path is shown in Fig. 3A (and the corresponding transition state is shown in fig. S1A). Unlike single flips, this double flip breaks one hydrogen bond. We call this the antigeared path because the H-1 atom rotates out of its hydrogen bond in the opposite sense to H-7 (which rotates in to form a hydrogen bond with O-A).

Because $P_a^2 = E$ (the identity), it follows that the antigeared path gives a simple doublet splitting pattern. Now, P_a is the only permutation that breaks no more than one hydrogen bond. Hence the observed pattern (Fig. 2A), in which the doublet is split further into six lines, implies that, unlike other water clusters, the PR1 hexamer supports tunneling paths that break two or more hydrogen bonds. In other water clusters, the next most feasible tunneling pathways after the flips are bifurcations, in which an H atom rotates away from its hydrogen bond and is replaced by the other H atom on the same water molecule (*15*). This mechanism breaks only one hydrogen bond in the trimer, but in PR1, owing to its three-dimensional structure, such a bifurcation rearrangement must break at least two hydrogen bonds. We located a variety of single-bifurcation tunneling pathways but found that, as in the water octamer (*39*), the resulting instanton tunneling splittings were tiny, indicating that these paths are unfeasible. However, we found that there exists a single feasible pathway that combines a double flip with a bifurcation, corresponding to the permutation $P_g = (AD)(BF)(CE)(1\,8\,2\,7)(3\,11)(4\,12)(5\,9)(6\,10)$. This path also breaks two hydrogen bonds, but surprisingly, the resulting instanton pathway (Fig. 3B) gives a small but observable tunneling splitting. This is because it describes a geared pathway, in which atoms H-1 and H-7 rotate in the same sense, resulting in a reduction in energy, which offsets the increase in energy required to break the additional H-2···O-B hydrogen bond.

The combination of both the geared and antigeared pathways explains the doublet-of-triplets splitting observed in the spectrum. P_a and P_g generate a group of permutations (described in the supplementary materials), which link together eight versions of the prism; Fig. 4A shows the graph that represents the connections between versions associated with these two tunneling pathways. To predict the splitting pattern, we must first obtain the energy levels by diagonalizing the tunneling matrix $\mathbf{h}$ (Fig. 4B), in which every connection in the graph is represented by a matrix element h_{ij} (where $i,j = 1, \ldots, 8$ label the versions). These elements were calculated using a normal-mode analysis of the ring-polymer instantons (*27*, *38*). Elements corresponding to a direct link by a single instanton path gave the values $h_a = -0.88$ MHz (antigeared) and $h_g = -0.15$ MHz (geared); all other permutations in the group were found to give negligibly small values of h_{ij}, which were thus set to zero. The resulting energy-level splitting obtained by diagonalizing the tunneling matrix is given in Fig. 4C. A symmetry analysis of the nonrigid cluster (*37*) shows that the eigenfunctions of the tunneling matrix transform as irreducible representations of a group isomorphic to the D_{2d} point group. We can therefore assign symmetry labels to the levels (Fig. 4C).

In the hexamer prism, the energy-level splittings caused by tunneling (on the order of megahertz) are significantly smaller than the energy separation for the rotational energy levels (several gigahertz). Therefore, it is appropriate to consider a tunneling energy level pattern for each different

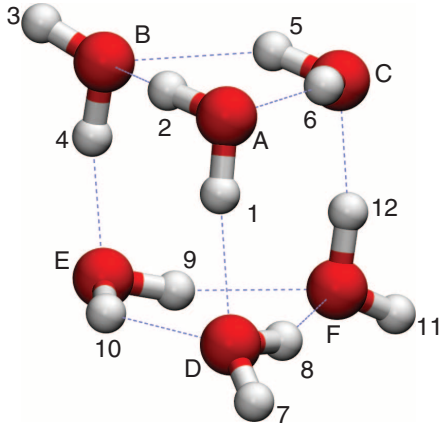

Fig. 1. Minimum-energy structure of the PR1 prism isomer of the water hexamer. The labels define one version (i.e., arrangement of the atoms), which can tunnel to other versions by permuting identical atomic nuclei within the structure.

[1]Department of Chemistry, University of Cambridge, Lensfield Road, Cambridge CB2 1EW, UK. [2]Department of Chemistry, Durham University, South Road, Durham DH1 3LE, UK. [3]Department of Chemistry, University of Virginia, McCormick Road, Charlottesville, VA 22903, USA. [4]Dean's Office, College of Arts and Sciences, and Department of Chemistry, Bucknell University, Lewisburg, PA 17837, USA. [5]Institute of Physics, Polish Academy of Sciences, Aleja Lotników 32/46, 02-668 Warszawa, Poland.
***Corresponding author. E-mail: jeremy.richardson@durham.ac.uk (J.O.R.); brookspate@virginia.edu (B.H.P.); sca10@cam.ac.uk (S.C.A.)** †Present address: Max Planck Institute for the Structure and Dynamics of Matter, Luruper Chausse 149, D-22761 Hamburg, Germany. ‡Present address: Department of Mathematics, Tonbridge School, High Street, Tonbridge, TN9 1JP, UK.

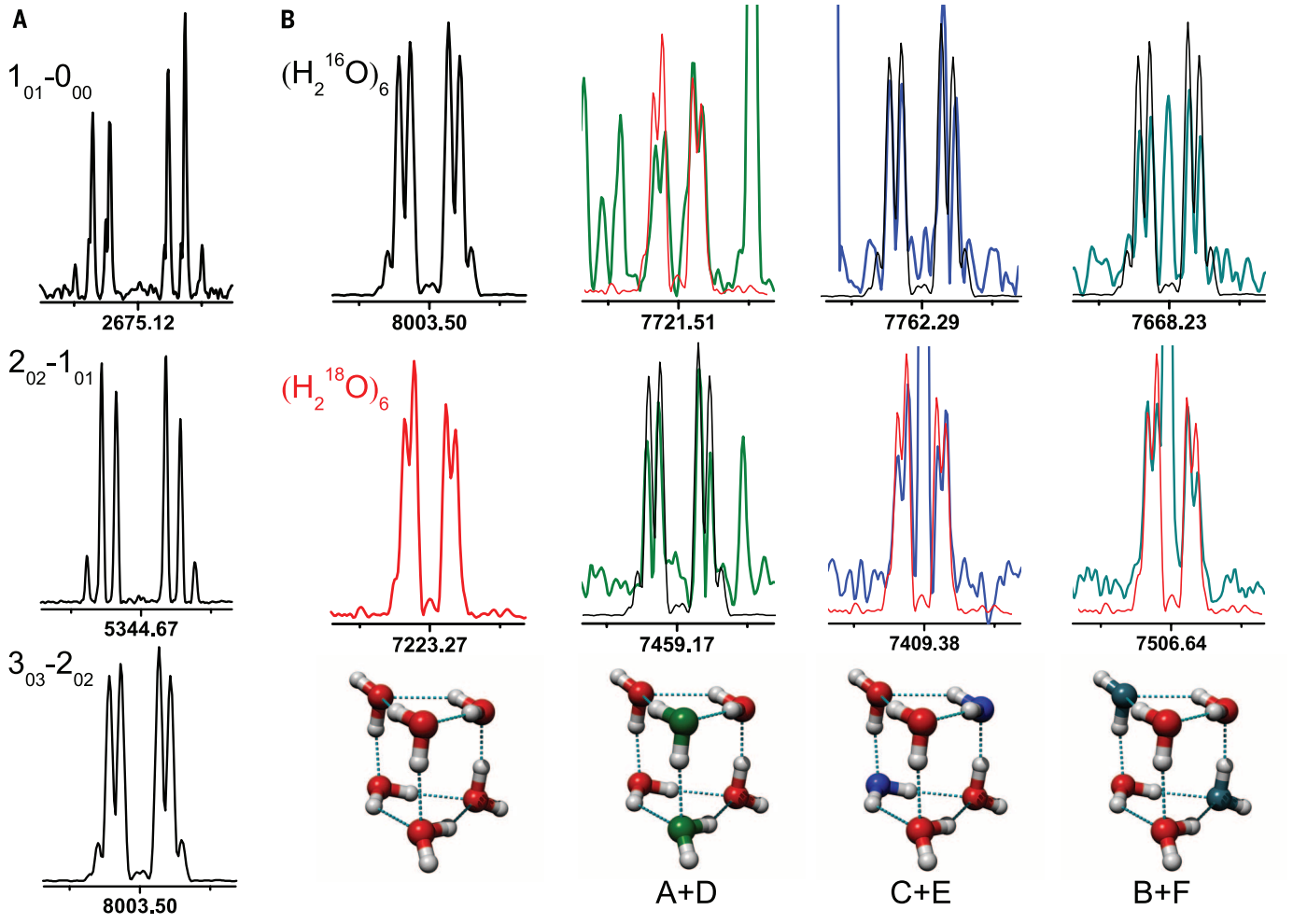

Fig. 2. Rotational spectral evidence for tunneling. (**A**) Three spectra for the $(H_2{}^{16}O)_6$ PR1 prism, showing the doublet-of-triplets splitting pattern attributed to tunneling. The rotational levels involved in each transition are denoted using the standard asymmetric top notation, $J_{K_aK_c}$. The labeled frequency is the asymmetric-top rotational transition frequency, and the tunneling pattern is symmetric around this frequency. (**B**) The 3_{03}–2_{02} spectra for the eight isotopologs (of 64 possible) that display tunneling. Tunneling is observed for both the $(H_2{}^{16}O)_6$ transition centered at 8003.50 MHz (black trace) and the $(H_2{}^{18}O)_6$ transition centered at 7223.27 MHz (red trace), and the width of the splitting pattern is reduced for the heavier isotopolog. The other isotopologs that show tunneling have either two $H_2{}^{18}O$ substitutions in the $(H_2{}^{16}O)_6$ structure (top row) or two $H_2{}^{16}O$ substitutions in the $(H_2{}^{18}O)_6$ cluster (bottom row). The substituted positions are depicted by the molecular structures at the bottom. All six of the doubly substituted clusters have a tunneling splitting (green and blue traces) that matches either the $(H_2{}^{16}O)_6$ or $(H_2{}^{18}O)_6$ clusters, as shown by the overlay of these spectra. All four spectra where water molecules A+D are $H_2{}^{16}O$ have the same, larger splitting (black trace), whereas all four clusters where A+D are $H_2{}^{18}O$ have the reduced tunneling splitting (red trace). The additional transitions observed in the doubly substituted spectra come from rotational transitions of other water cluster isotopologs and are not part of the tunneling-splitting pattern. The tick marks in all panels have 1-MHz spacing.

rotational level; these patterns can have a slight dependence on the rotational quantum numbers, as suggested by Fig. 2A. To obtain the splitting pattern in the rotational spectrum that consists of transitions between the tunneling states for different rotational levels, we note that μ_a transforms as B_2 and only allows strong transitions between the tunneling states $A_1 \leftrightarrow B_2$, $A_2 \leftrightarrow B_1$, and $E_{(1)} \leftrightarrow E_{(2)}$. These transitions give the doublet-of-triplet splitting pattern shown in Fig. 4D, and the amplitudes of the pattern are obtained from the nuclear-spin statistics. As explained in the supplementary materials, there are also some pure rotational transitions, which are not rigorously forbidden by symmetry but contribute only weakly to a small central peak, and evidence of these nominally forbidden transitions appears in Fig. 2. As shown in Fig. 4D, the theoretical splitting pattern qualitatively reproduces the experimentally observed splitting pattern but is about twice as wide. An analysis of the *J*-dependent geared and antigeared tunneling matrix elements, presented in the supplementary materials, gives the values of $h_a = -0.382$ MHz and $h_g = -0.073$ MHz for the ground state, which can be compared directly to the theoretical values given above. The ratio of the theoretical matrix elements $h_g : h_a$ is 1 : 5.8 and in excellent agreement with the experimental value of 1 : 5.2. Furthermore, full isotopic substitution of ^{16}O with ^{18}O is found to reduce the predicted tunneling matrix elements to 85% of their value, indicating a slight participation of the heavy oxygen-atom framework during tunneling. This is confirmed by the experimental tunneling splittings (Fig. 2B), which are proportional to the tunneling matrix elements, where the observed reduction is 84%. This level of agreement is good for an instanton calculation and is consistent with previous applications to other water clusters (*27*, *39*), where the main errors in the instanton calculation were attributed to neglect of anharmonicity in the fluctuations around the instanton, along with rotation-tunneling coupling. This implies that the potential energy surfaces give an excellent description of the intermolecular forces, and we can be confident that the geared and antigeared tunneling pathways in Fig. 3 correctly describe the tunneling responsible for the observed splittings.

Plots of the potential energy along the tunneling paths (Fig. 3) show striking differences between

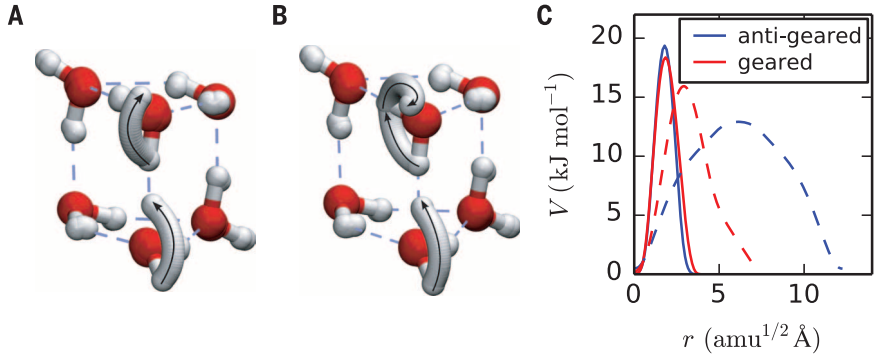

Fig. 3. Instanton tunneling pathways in the water hexamer prism. (**A**) Antigeared and (**B**) geared variations. The pathways are shown as conflated snapshots of replicas of the system obtained from ring-polymer representations of the instantons. The geared pathway involves the concerted breaking of two hydrogen bonds. (**C**) Variation of the potential energy along the instanton paths (solid lines) and minimum-energy paths (dashed lines), where r is the integrated mass-weighted path length and V is the potential energy along the path.

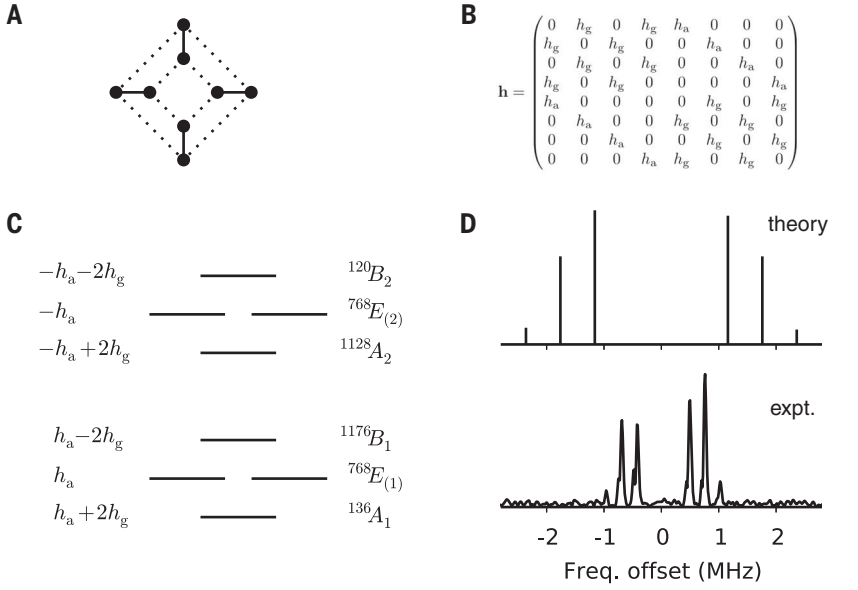

Fig. 4. Origin of the splitting pattern. (**A**) Graph showing how the versions (vertices) are connected by the tunneling paths (antigeared, solid lines; geared, dotted lines). Diagonalization of the associated tunneling matrix, $\mathbf{h}$, defined in (**B**) splits the ground-state energy level as shown in (**C**), where the symmetry is also given with its nuclear-spin degeneracy as a superscript. The states labeled $E_{(1)}$ and $E_{(2)}$ both have symmetry E. The rotational spectrum involves transitions between the tunneling-level patterns for different rotational energy levels. The resulting tunneling-splitting pattern centered on the expected rotational transition frequency is $2h_a + 4h_g$, $2h_a$, $2h_a-4h_g$, $-2h_a + 4h_g$, $-2h_a$, $-2h_a-4h_g$, where h_a and h_g are the average values of the antigeared and geared tunneling matrix elements in the rotational energy levels for the spectroscopic transition. This spectral pattern is plotted in (**D**) using the theoretical matrix elements as the average values in the rotational levels and is compared with the measured 1_{01}–0_{00} transition (represented to scale). This explains the observed doublet-of-triplets splitting pattern, where the outermost lines are considerably smaller.

the instanton and minimum-energy paths. The mass-weighted length of the minimum-energy path is four times that of the instanton path for the antigeared pathway and twice that for the geared. A naïve one-dimensional analysis using the minimum-energy paths might conclude that the geared tunneling is more facile than the antigeared (because the effective barrier is much thinner), and that in either case the splitting pattern is probably too small to be observed on account of the long tunneling pathways. That the splittings are observable and that the ratio is the other way around are the result of corner-cutting by the instanton pathway (*40*). Unlike the minimum-energy path, it bypasses the transition state in order to avoid the penalty in the action associated with moving the heavy oxygen atoms.

It is likely that other prism clusters, such as the pentagonal prism decamer, could exhibit similar pathways. These results also raise the possibility that the rearrangement dynamics of water in interfacial (*41*, *42*) or confined environments might also involve similar concerted breaking of two (or more) hydrogen bonds.

REFERENCES AND NOTES

1. A. C. Legon, D. J. Millen, *Chem. Soc. Rev.* **21**, 71 (1992).
2. N. Pugliano, R. J. Saykally, *Science* **257**, 1937–1940 (1992).
3. R. J. Saykally, G. A. Blake, *Science* **259**, 1570–1575 (1993).
4. K. Liu, J. D. Cruzan, R. J. Saykally, *Science* **271**, 929–933 (1996).
5. F. N. Keutsch, R. J. Saykally, *Proc. Natl. Acad. Sci. U.S.A.* **98**, 10533–10540 (2001).
6. C. Pérez *et al.*, *Science* **336**, 897–901 (2012).
7. R. J. Saykally, D. J. Wales, *Science* **336**, 814–815 (2012).
8. C. Pérez *et al.*, *Chem. Phys. Lett.* **571**, 1–15 (2013).
9. C. Pérez *et al.*, *Angew. Chem. Int. Ed.* **53**, 14368–14372 (2014).
10. S. C. Althorpe, D. C. Clary, *J. Chem. Phys.* **101**, 3603 (1994).
11. D. Sabo, Z. Bačić, T. Bürgi, S. Leutwyler, *Chem. Phys. Lett.* **244**, 283–294 (1995).
12. K. Liu *et al.*, *Nature* **381**, 501–503 (1996).
13. K. Liu, M. G. Brown, R. J. Saykally, *J. Phys. Chem. A* **101**, 8995–9010 (1997).
14. D. J. Wales, *Theory of Atomic and Molecular Clusters: With a Glimpse at Experiments*, J. Jellinek, Ed. (Springer-Verlag, Berlin, 1999), pp. 86–110.
15. D. J. Wales, *J. Am. Chem. Soc.* **115**, 11180–11190 (1993).
16. T. R. Walsh, D. J. Wales, *J. Chem. Soc., Faraday Trans.* **92**, 2505 (1996).
17. D. J. Wales, T. R. Walsh, *J. Chem. Phys.* **105**, 6957 (1996).
18. D. J. Wales, T. R. Walsh, *J. Chem. Phys.* **106**, 7193 (1997).
19. J. K. Gregory, D. C. Clary, *J. Chem. Phys.* **103**, 8924 (1995).
20. J. K. Gregory, D. C. Clary, *J. Chem. Phys.* **102**, 7817 (1995).
21. J. K. Gregory, D. C. Clary, *J. Phys. Chem. A* **101**, 6813–6819 (1997).
22. E. H. T. Olthof, A. van der Avoird, P. E. S. Wormer, K. Liu, R. J. Saykally, *J. Chem. Phys.* **105**, 8051 (1996).
23. C. Leforestier, L. B. Braly, K. Liu, M. J. Elrod, R. J. Saykally, *J. Chem. Phys.* **106**, 8527 (1997).
24. R. S. Fellers, L. B. Braly, R. J. Saykally, C. Leforestier, *J. Chem. Phys.* **110**, 6306 (1999).
25. R. Bukowski, K. Szalewicz, G. C. Groenenboom, A. van der Avoird, *Science* **315**, 1249–1252 (2007).
26. X. Huang *et al.*, *J. Chem. Phys.* **128**, 034312 (2008).
27. J. O. Richardson, S. C. Althorpe, D. J. Wales, *J. Chem. Phys.* **135**, 124109 (2011).
28. U. Góra, R. Podeszwa, W. Cencek, K. Szalewicz, *J. Chem. Phys.* **135**, 224102 (2011).
29. Y. Wang, B. C. Shepler, B. J. Braams, J. M. Bowman, *J. Chem. Phys.* **131**, 054511 (2009).
30. Y. Wang, X. Huang, B. C. Shepler, B. J. Braams, J. M. Bowman, *J. Chem. Phys.* **134**, 094509 (2011).
31. V. Babin, G. R. Medders, F. Paesani, *J. Phys. Chem. Lett.* **3**, 3765–3769 (2012).
32. V. Babin, G. R. Medders, F. Paesani, *J. Chem. Theory Comput.* **10**, 1599–1607 (2014).
33. F. N. Keutsch, J. D. Cruzan, R. J. Saykally, *Chem. Rev.* **103**, 2533–2578 (2003).
34. B. Temelso, K. A. Archer, G. C. Shields, *J. Phys. Chem. A* **115**, 12034–12046 (2011).
35. Y. Wang, V. Babin, J. M. Bowman, F. Paesani, *J. Am. Chem. Soc.* **134**, 11116–11119 (2012).
36. V. Babin, F. Paesani, *Chem. Phys. Lett.* **580**, 1–8 (2013).
37. H. C. Longuet-Higgins, *Mol. Phys.* **6**, 445–460 (1963).
38. J. O. Richardson, S. C. Althorpe, *J. Chem. Phys.* **134**, 054109 (2011).
39. J. O. Richardson *et al.*, *J. Phys. Chem. A* **117**, 6960–6966 (2013).
40. S. Chapman, B. C. Garrett, W. H. Miller, *J. Chem. Phys.* **63**, 2710 (1975).
41. T. Mitsui, M. K. Rose, E. Fomin, D. F. Ogletree, M. Salmeron, *Science* **297**, 1850–1852 (2002).
42. V. A. Ranea *et al.*, *Phys. Rev. Lett.* **92**, 136104 (2004).

ACKNOWLEDGMENTS

The authors acknowledge financial support from a European Union COFUND/Durham Junior Research Fellowship (J.O.R.), a Research Fellowship from the Alexander von Humboldt Foundation (C.P.), U.S. National Science Foundation grants CHE-0960074 (C.P. and B.H.P.) and CHE-1213521 and CHE-1229354 (B.T. and G.C.S.), Swiss National Science Foundation grant PBBEP2-144907 (S.L.), the UK Engineering and Physical Sciences Research Council (J.O.R., A.A.R., D.J.W., and S.C.A.), and a grant from the Polish National Science Centre, decision number DEC/2011/02/A/ST2/00298 (Z.K.).

SUPPLEMENTARY MATERIALS

www.sciencemag.org/content/351/6279/1310/suppl/DC1
Materials and Methods
Figs. S1 to S9
Tables S1 to S74
References (*43*–*66*)

6 December 2015; accepted 2 February 2016
10.1126/science.aae0012

Concerted hydrogen-bond breaking by quantum tunneling in the water hexamer prism

Jeremy O. Richardson *et al.*

Science **351**, 1310 (2016);
DOI: 10.1126/science.aae0012